DEBRIS FLOW NETWORK MORPHOLOGY AND A NEW EROSION RATE PROXY FOR STEEPLAND BASINS WITH APPLICATION TO THE OREGON COAST RANGE AND CASCADIA SUBDUCTION ZONE

by

BRIAN DANIEL PENSERINI

A THESIS

Presented to the Department of Geological Sciences
and the Graduate School of the University of Oregon
in partial fulfillment of the requirements
for the degree of
Master of Science

June 2015

THESIS APPROVAL PAGE

Student: Brian Daniel Penserini

Title: Debris Flow Network Morphology and a New Erosion Rate Proxy for Steepland Basins with Application to the Oregon Coast Range and Cascadia Subduction Zone

This thesis has been accepted and approved in partial fulfillment of the requirements for the Master of Science degree in the Department of Geological Sciences by:

Joshua Roering	Chairperson
Rebecca Dorsey	Member
Mark Fonstad	Member

and

Scott L. Pratt	Dean of the Graduate School

Original approval signatures are on file with the University of Oregon Graduate School.

Degree awarded June 2015

THESIS ABSTRACT

Brian Daniel Penserini

Master of Science

Department of Geological Sciences

June 2015

Title: Debris Flow Network Morphology and a New Erosion Rate Proxy for Steepland Basins with Application to the Oregon Coast Range and Cascadia Subduction Zone

Reaches dominated by debris flow scour and incision tend to greatly influence landscape form in steepland basins. Debris flow networks, despite their ubiquity, have not been exploited to develop erosion rate proxies. To bridge this gap, I applied a proposed empirical function that describes the variation of valley slope with drainage area in fluvial and debris flow reaches of steepland channel networks in the Oregon Coast Range. I calibrated a relationship between profile concavity and erosion rate to map spatial patterns of long-term uplift rates assuming steady state. I also estimated the magnitude and inland extent of coseismic subsidence in my study area. My estimates agree with field measurements in the same area along the Cascadia margin, indicating that debris flow valley profiles can be used to make interpretations from spatial patterns of rock uplift that may better constrain physical models of crustal deformation.

This thesis includes unpublished co-authored material.

CURRICULUM VITAE

NAME OF AUTHOR: Brian Daniel Penserini

GRADUATE AND UNDERGRADUATE SCHOOLS ATTENDED:

University of Oregon, Eugene, OR
California Institute of Technology, Pasadena, CA

DEGREES AWARDED:

Master of Science, Geological Sciences, 2015, University of Oregon
Bachelor of Science, Geology, 2013, California Institute of Technology

AREAS OF SPECIAL INTEREST:

Geomorphology and Surface Processes

PROFESSIONAL EXPERIENCE:

Graduate Teaching Fellow, University of Oregon
September 2013-June 2015

Undergraduate Teaching Assistant, California Institute of Technology
April 2013-June 2013

Summer Undergraduate Research Fellow, California Institute of Technology
July 2012-September 2012

ACKNOWLEDGMENTS

I would like to express my sincere appreciation to Professor Roering for his assistance in the preparation of this manuscript and guidance throughout this project. In addition, special thanks are due to Professors Dorsey and Fonstad for their recommendations and editing help.

TABLE OF CONTENTS

Chapter Page

LIST OF FIGURES

LIST OF TABLES

Table Page

CHAPTER I

INTRODUCTION

The following chapter (Chapter II) is an inclusive work documenting the entirety of the research I completed for fulfillment of the requirements for the degree of Master of Science in Geological Sciences. Chapter II will be submitted for publication with Josh Roering as a co-author, however I completed the entirety of the work independently.

CHAPTER II

DEBRIS FLOW MORPHOLOGY AND A NEW EROSION RATE PROXY FOR STEEPLAND BASINS WITH APPLICATION TO THE OREGON COAST RANGE AND CASCADIA SUBDUCTION ZONE

The work described in this chapter was conducted entirely by myself. Josh Roering provided editing help and will be listed as a co-author upon submission for publication, however I did all of the writing. The following chapter is presented in the style of the journal *Earth and Planetary Science Letters*.

1. Introduction

Changes in base level driven by relative rock uplift rate influence the shape of river profiles as the channel network responds to newly imposed boundary conditions. When steady state conditions have been attained, these graded streams have channel slopes that are adjusted to the minimum allowed slope to accommodate the transport of supplied material and incise bedrock at a pace commensurate to rock uplift (Mackin, 1948; Whipple and Tucker, 1999). As a result, slope angles in adjusted channel reaches tend to decrease downstream as stream discharge increases and sediment grain size decreases. This forms a concave profile, the shape of which can be examined to extract information on the rate of base level change (Kirby and Whipple, 2001; Wobus et al., 2006a). For example, if the rate of base level fall were to suddenly increase to a new value, channel slopes would steepen in response to the change in boundary condition and over time a new equilibrium long profile would be formed. By comparing the shapes of

the different equilibrium long profiles, one can extract information about rock uplift rate (Hack, 1973; Kirby and Whipple, 2001; Perron and Royden, 2013; Wobus et al., 2006a).

However in addition to rock uplift rate, climate and lithology also influence the amount of sediment supplied to stream channels and the ability of a stream to transport that material, which in turn dictates the shape of the long profile. Furthermore, spatial or temporal variations in these factors may lead to segmented profiles that are controlled by locally imposed boundary conditions (i.e. knickpoints). In practice, it is difficult to deconvolve the relative influences of uplift rate, climate, and lithology on channel profile form without additional constraints on these factors. Therefore, analysis of long profiles to extract variations in rock uplift rate requires that lithology and climate are relatively constant over the study region, or at least insignificantly variable.

The stream power law is a geomorphic transport law, a functional relationship that relates landscape form to erosion process, that allows spatial variations in relative rock uplift to be inferred from an examination of fluvial long profiles (Ahnert, 1970; Binnie et al., 2007; Dietrich et al., 2003; Howard and Kerby, 1983; Milliman and Syvitski, 1992). It is built on the assumption that the incision rate along a channel bed is a function of the shear stress, or alternatively the unit stream power, acting on the channel bed (Howard and Kerby, 1983; Whipple and Tucker, 1999). The general form of the stream power law states that incision rate is equivalent to the power law product of channel slope and drainage area (Whipple, 2004). For equilibrated channel profiles, where uplift and incision rates are balanced, the stream power law reduces to an inverse power law relationship between channel slope and drainage area. In a recent review paper, Kirby and Whipple (2012) summarize and synthesize existing studies that have

used the stream power law to make tectonic interpretations. They describe the following three case studies: measuring differential rock uplift across a fault-bend fold in the Siwalik Hills (Hurtrez et al., 1999; Kirby and Whipple, 2001; Lague and Davy, 2003), determining how abruptly rock uplift rate increases from the Lesser to Higher Himalaya (Kirby and Ouimet, 2011; Kirby et al., 2003; Wobus et al., 2003; Wobus et al., 2006b), and inferring tectonic history from the geomorphic response to fault throw in eastern California (Whittaker et al., 2007).

While the stream power law has proven to be an effective reconnaissance tool for detecting spatial and temporal variations in deformation, its scope is limited by the fact that it applies to only to fluvial river channels. Because the stream power law integrates upstream areas, it is difficult to uniquely associate rock uplift rate variations implied by changing values of channel steepness in a spatially explicit fashion. Upstream of the fluvial-dominated regime of most mountainous areas, debris flow scour is the dominant sediment transport and incision process (Benda, 1990; Dietrich and Dunne, 1978; Stock and Dietrich, 2003). These debris flow-dominated reaches are typically found at relatively small drainage areas (<0.1-1 km^2), where topography is convergent but fluvial features indicative of channelization are absent (Stock and Dietrich 2003) (Figure 1). Termed colluvial valleys (Montgomery and Buffington, 1997), these reaches represent the transition from hillslopes to the channelized portion of the landscape and are zones of accumulation of coarse, unconsolidated material that can mobilize debris flows.

The morphology of debris flow reaches deviates significantly from the characteristic concave profile of fluvial networks. Longitudinal profiles of debris flow-dominated reaches tend to be steeper and less concave, approaching a constant slope at

very small drainage areas (~10^3 m^2), coincident with unchanneled valleys. It has been proposed that these colluvial reaches are simply described by a separate inverse power law relationship (Lague and Davy, 2003; Whipple and Tucker, 1999), however the advent of high-resolution laser altimetry has enabled resolution of a curved log-log slope-area relation for debris flow valleys (Stock and Dietrich, 2003; Stock and Dietrich, 2006). Hypothetically, this curved relation could be approximated by numerous power law relationships, each describing a separate debris flow valley long-profile, but this approach lacks a physical, mechanistic basis and is not supported by field evidence (Stock and Dietrich, 2006). While investigating the topographic signature of debris flows at small drainage areas in steepland landscapes, Stock and Dietrich (2003) developed an empirical function to describe the shape of valley slope-area data in these reaches. Their relatively simple function describes the transition from the constant slope morphology seen at small drainage areas to the inverse power law relationship of fluvial channels at larger drainage areas. Using their function to describe the form of debris flow valleys worldwide, Stock and Dietrich (2003) documented that as erosion rates increased for a given lithology, the profile of debris flow valleys became increasingly linear, forcing the transition from debris flow to fluvial dominated reaches to occur more abruptly.

Given topographic data of sufficient resolution, debris flow catchments have the potential to serve as local recorders of rock uplift rate as their valley profiles are influenced by local base level. Hurtrez et al. (1999) observed a correlation between relief and uplift rate at length scales shorter than 600m, implying that colluvial valleys adjust to tectonically driven changes in base level. The relatively small size of debris flow catchments, as compared to large downstream, integrated fluvial networks, highlights the

possibility of mapping base level (and thus rock uplift rate) from profile form in a spatially extensive fashion. This poses the following question: Can the shape of debris flow valley profiles and transitional reaches be used to interpret patterns of rock uplift rate in active orogens?

Figure 1: Debris Flow Catchments. This image shows characteristic debris flow dominated catchments in the Oregon Coast Range. The drainage network originates near the ridgecrests at colluvial hollows, where sediment accumulates over time. Evacuation of accumulated sediment and debris by shallow landsliding during large storm events trigger debris flows, which traverse the network and scour to bedrock.

In convergent settings (i.e. active margins), uplift is typically punctuated by earthquakes that release the elastic strain accumulated during interseismic periods of the earthquake cycle. Observations of pre- and coseismic deformation before and after the 1946 M=8 earthquake in the Nankai Trough of Southwest Japan indicates that coseismic displacement recovers the majority of accumulated interseismic strain, but the existence of topography suggests that some amount of permanent strain accumulates (Hyndman

and Wang, 1995). Most generally, coastlines along active margins distinguish the boundary between regions of long-term net relative uplift and regions of long-term net relative subsidence or zero net relative elevation change. However, it is unclear how rapidly this transition occurs in coastal areas and therefore it is uncertain how far increasing long-term uplift rates extend into the coastal margin of mountain ranges where changes in uplift and sea level control base level changes. Given these complications in near coastal settings, few studies have attempted to reconcile earthquake deformation with long-term rock uplift rates, so the relative contribution of deformation associated with the earthquake deformation cycle in the long-term uplift of these environments is poorly constrained. By combining uplift rate patterns from an analysis of debris flow valley profiles in coastal active orogens with the spatial pattern of interseismic deformation rates, it may be possible to distinguish the relative contribution of coseismic and interseismic deformation along the margins of active orogens.

The Cascadia Subduction Zone is a well-studied active margin that experiences significant coseismic deformation along coastal regions from Oregon to British Columbia. Since the last major megathrust rupture along its margin in 1700 AD, most coastal areas in this region have experienced interseismic uplift that exceeds rates of long-term rock uplift and erosion. Along the Oregon Coast lies the Oregon Coast Range (OCR), an active orogen believed to be sustained, at least in part, by uplift induced by inelastic strain caused by the convergence of the Juan de Fuca Plate on the North American Plate. We focused our analysis on the central OCR, a well-documented steepland landscape with consistent bedrock and climate, and applied the empirical function of Stock and Dietrich (2003) to numerous small (<10 km^2) debris flow-

dominated catchments proximal to the coast (Figure 1). Using several cosmogenic radionuclide-derived catchment average erosion rates, we developed a function that relates debris flow valley form to erosion rate. By applying this erosion rate function to our study catchments, we were able to map long-term uplift rate estimates in the central OCR. By comparing the pattern of long-term uplift rates to the pattern of current uplift rates derived from leveling surveys, we estimated coseismic subsidence attributable to Cascadia megathrust earthquakes.

2. Theory

2.1. Fluvial Channel Model

Fluvial channels typically exist at drainage areas greater than 0.1-1.0 km^2, where valley slopes are less than 0.03-0.10 (Stock and Dietrich, 2003). The relationship between incision rate, channel slope, and drainage area in these reaches is often expressed by the general form of the stream power law:

$$E = KA^m S^n$$

where E is the rate of bedrock channel incision, K is the erosion coefficient, A is drainage area, S is local channel slope, and m and n are empirically derived constants (Whipple, 2004) (parameters and variables discussed herein are listed in the Table 1 in Appendix A). This form of the stream power law is practical since it is formulated in terms of local channel slope and upstream drainage area, two parameters that are easily estimated from digital elevation models (DEMs). Furthermore for a landscape in steady state, the stream power model can be rewritten as Flint's Law (Flint, 1974):

$$\frac{dz}{dt} = U - E = U - KA^m S^n = 0$$

$$U = KA^m S^n$$

$$S = \left(\frac{U}{K}\right)^{\frac{1}{n}} A^{-\frac{m}{n}}$$

$$S = k_s A^{-\theta}$$

where $\frac{dz}{dt}$ is the rate of change of the bed elevation, U is the relative rock uplift rate, $k_s = \left(\frac{U}{K}\right)^{\frac{1}{n}}$ and is referred to as the channel steepness index with units (length$^{2\theta}$) (Snyder et al. 2000), and $\theta = \frac{m}{n}$ and is referred to as the concavity index, which is unitless. This form of the stream power law demonstrates an inverse power law relationship between drainage area and channel slope that produces a linear trend in log-log slope-area space, as long as equilibrium conditions are met and K is constant. Studies that have examined the variability of both k_s and θ between different catchments with uplift rate being the only variable and these studies indicate that θ does not systematically vary with uplift rate. Meanwhile, k_s is very sensitive to changes in uplift (Duvall et al., 2004; Kirby and Whipple, 2001; Lague et al., 2000; Snyder et al., 2000). Since the units of channel steepness index depend on the corresponding θ value, a fixed value of θ called the reference concavity, θ_{ref}, is used in order to compare steepness indices between profiles. The steepness index that results from the best fitting power law with $\theta = \theta_{ref}$ is called the normalized channel steepness index, k_{sn}. This has led to the formulation of many linear and nonlinear relationships between incision rate and normalized channel steepness, which can be used to estimate uplift rate variations across a given landscape assuming all else equal (Binnie et al., 2007; Cyr et al., 2010; DiBiase et al., 2010; Duvall et al., 2004;

Harkins et al., 2007; Kirby and Whipple, 2001; Kirby and Whipple, 2012; Koons and Kirby, 2007; Lague and Davy, 2003; Ouimet et al., 2009; Snyder et al., 2000, 2003a, b; Whipple and Tucker, 1999; Wobus et al., 2006a).

2.2. Debris Flow Valley Model

At drainage areas lower than 0.1-1.0 km^2, the relationship between slope and area deviates from the power law trend associated with fluvial regions. Unlike the linear relation demonstrated by fluvial reaches, these reaches are described by a curved relationship in log-log slope-area space, representing a scaling break from the log-log linear stream power relationship (Stock and Dietrich, 2003; Stock and Dietrich, 2006). The function proposed by Stock and Dietrich (2003) to fit the slope-area relationship for debris flow valleys is as follows:

$$S = \frac{s_0}{1 + a_1 A^{a_2}}$$

where s_0 is an empirical constant with units of (length/length) that represents valley head slope (slope at negligible drainage area), a_1 is an empirical constant (with units of $1/(length^2)^{a2}$) that is inversely proportional to the curvature of the relationship and represents the sharpness of the transition is in slope-area space and in profile, and a_2 is a unitless empirical constant that is analogous to θ in the sense that it represents a power law slope at large drainage areas (Stock and Dietrich, 2003). Stock and Dietrich (2003) recognized that these three parameters can account for curved slope-area relationships from debris flow dominated reaches in diverse geologic settings. This function condenses to a constant slope ($S \sim s_0$) at small drainage areas and to an inverse power law, similar to the stream power law, at large drainage areas ($S \sim \frac{s_0}{a_1} A^{-a_2}$), thus emulating the transition

between regimes that we see in real slope-area data. Because s_0 is theoretically controlled by shallow landslide mechanics in colluvial hollows, it may not vary dramatically with uplift (or erosion) rate. Additionally, a_2 is not believed to vary with uplift/erosion rate assuming that basin geometry and erosional process remains constant.

Stock and Dietrich (2003) inferred a potential correlation between a_1, which can be conceptualized as the convexity of the transition between the debris flow and fluvial portions of slope-area relationships, and both rock uplift rate and lithology. Using data collected from 12 regions of similar lithology in the U.S. they note that as uplift rate increases, there is a propensity for a_1 to decrease and, thus, curvature of the slope-area relation to increase (Figure 2). They hypothesize that as uplift rate increases, lower threshold slopes migrate to larger drainage areas in a manner similar to the responses of fluvial systems in the models of Howard (1997) and Tucker and Bras (1998) (Stock and Dietrich, 2003). Debris flow valley slopes at small drainage areas are relatively invariant due to landslide initiation mechanics at values close to the friction angle of soil (Stock and Dietrich, 2003). Further down the network, valley slopes begin to decrease as the sublinear debris flow dominated reaches transition to channelized fluvial reaches. Debris flows in the confined valleys of this transitional realm tend to deposit at slopes of ~0.03-0.1 as they are unable to overcome the forces resisting downslope movement (Stock and Dietrich, 2003; Stock and Dietrich, 2006). This physical limit marks the lower extent of the curved slope-area relation and likely remains unchanged with increasing uplift rate. Therefore increasing rock uplift rate potentially shifts debris flow valley slopes to greater drainage areas, which effectively concentrates long-profile and slope-area curvature

downstream and produces a more abrupt transition that is reflected by lower a_1 values (Figure 2).

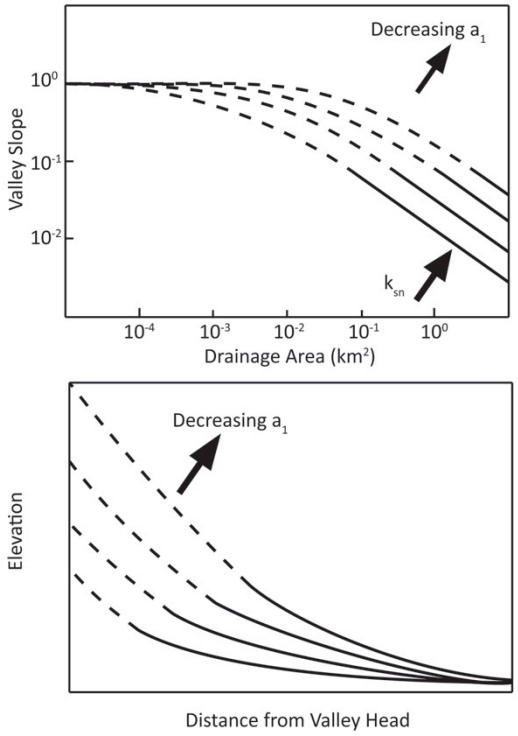

Figure 2: a1 Variation Plots. The top figure demonstrates the response of increasing a_1, all else being equal. Dashed curves represent the debris flow dominated portion of the network while solid lines represent the fluvial portion. All curves converge to the upper threshold slope controlled theoretically by shallow landsliding and represented by s_0. The slope at which debris flows are deposited marks the down-network extent of the debris flow dominated reaches and serves as a lower threshold that debris flows are physically unable to travel beyond. The lower figure shows the approximate corresponding valley profiles with debris flow reaches characterized primarily by a more linear shape.

3. Regional Context

The OCR is a humid, unglaciated, forested, soil-mantled, mountainous landscape characterized by steep topography and relatively evenly spaced ridges and valleys. The bedrock of the central OCR is largely composed of the Eocene Tyee Formation, a ~3 km

thick, sand-rich sequence of turbidites with gently dipping, undeformed strata of relatively uniform lithology (Baldwin, 1956; Dietrich and Dunne, 1978; Heller and Dickinson, 1985; Reneau and Dietrich, 1991; Snavely et al., 1964). East-west facies variability is minimal, but there exists a south to north reduction in formation thickness and sandstone to siltstone ratio due to the orientation of the delta-fed submarine margin at the time of deposition (Heller and Dickinson, 1985; Lovell, 1969). Uplift of the OCR was initiated in the Miocene and is driven by subduction of the Juan de Fuca plate at the offshore Cascadia Subduction Zone, located 60-100 km west of the Oregon coast (McNeill et al., 2000). Positive net uplift continues today as evidenced by prominent wave-cut platforms with long-term rates ranging from 0.1-0.3 mm/yr along the central Oregon coast from Newport to Coos Bay (Kelsey et al., 1996). Additionally, long-term uplift rates derived from measurements of strath terraces throughout the central OCR also range from 0.1-0.3 mm/yr, indicating spatially uniform long-term uplift rates throughout the central OCR (Personius, 1995). Local structures account for the majority of the variability in both of these measures.

Erosion rate estimates derived from several methods, including suspended sediment yield, colluvial sediment flux, cosmogenic radionuclides, and radiocarbon, suggest long-term values of around 0.1 mm/yr throughout the central OCR (Beschta, 1978; Bierman et al., 2001; Heimsath et al., 2001; Reneau and Dietrich, 1991). This agreement between long-term uplift and erosion rates implies that the central OCR is an approximate steady state landscape over timescales of 10^4-10^5 years as the estimated characteristic hillslope adjustment timescale is 50 kyr (Roering et al., 2001). However despite this apparent balance, there exists local, small-scale transience (both temporally

and spatially) in the form of deep-seated landslides, drainage capture and reorganization, and differential stream incision associated with rock strength variations and bedrock meandering (Almond et al., 2007; Roering et al., 2005).

In the OCR, reaches dominated by debris flow scour and incision tend to substantially influence landscape form as they account for >80% of network length as well as the vast majority of valley network relief (Benda and Dunne, 1997). Debris flow runouts tend to stop upstream of channel slopes of ~0.03-0.1, where step-pool bed forms begin to appear and long-term fluvial processes become dominant (Montgomery and Buffington, 1997; Stock and Dietrich, 2006). In the OCR, these slopes tend to correspond with the aforementioned slope-area scaling break at 0.1-1.0 km^2 that is typical for steepland areas. Below this scaling break lies the fluvial-dominated portion of the channel network, however the extent of the fluvial regime is limited by the appearance of alluvial processes that can emerge at areas of ~3 km^2 in many coastal catchments.

4. Methods

4.1. Topographic Analysis

The Oregon Coast Range serves as an ideal testing ground for a method to extract incision rate information from debris flow-dominated catchment valley profiles due to the prevalence of debris flow dominated reaches, relatively uniform lithology and climate, and an approximate balance between long-term uplift and erosion rates. Using high-resolution 1m airborne laser altimetry (Lidar) data provided by the Oregon Department of Geology and Mineral Industries (DOGAMI), we fit the empirical function of Stock and Dietrich (2003) to a study group of 83 catchments between 0.4 and 3.0 km^2. We selected

catchments from a region near the outlet of the Umpqua River to the North, South, and East of the town of Reedsport (Figure 3). This area is void of major faults and has minimal folding. The major anticline that runs approximately N-S through our study area is gentle with dips of ~4-6° away from the fold (Marshall and Roering, 2014). We assume that the mapped folds in our study area do not influence topography since anticlinal structures in the Tyee Formation do not lead to elevated relief (Marshall and Roering, 2014). We attempted to avoid selecting catchments where base level is influenced by transient features, such as large scale lithologic knickpoints and deep-seated landslides. We extracted the valley network from each catchment using TopoToolbox 2, a MATLAB based geoprocessing toolbox, and with a minimum drainage area of 250 m^2 (Schwanghart and Scherler, 2013). This threshold corresponds to the downslope extent of the hillslope regime and the onset of shallow landsliding in topographic hollows (Roering, 2008). Valley network elevations were then smoothed[1] using a 15m smoothing window with a first-order Savitzky-Golay filter and local slopes and drainage areas were calculated from the smoothed network (Roering et al., 2010). Slope and area values were log-transformed and subsequently binned to reduce the overwhelming number of data points in each catchment and reduce scatter[2]. The smoothed, log-transformed, and binned slope-area values were then fit with the empirical function proposed by Stock and Dietrich (2003) using the MATLAB Curve Fitting Toolbox. Each point was weighted by the number of measurements included in each bin, which weights each pixel along the profiles equally (Stock and Dietrich, 2003). Data points with channel gradients less than 0.03, the lower slope limit at which debris flows

[1] ChannelSmoother code generously provided by Scott Miller.

[2] Binning code generously provided by Taylor Perron.

tend to deposit in the OCR (Stock and Dietrich, 2003), were eliminated to isolate the fit to debris flow-dominated and transitional reaches. Best fitting parameters (a_1, a_2, and s_0) for each catchment, as well as 95% confidence intervals, degrees of freedom, and R^2 values, were recorded. We retained catchments that had R^2 values greater than 0.85 in order to eliminate obviously anomalous catchments that contained transient influences or a lack of debris flow processes that led to anomalous best-fitting model parameters. Since a single threshold could not precisely differentiate between catchments with and without transience, we inspected valley profiles of the remaining catchments and eliminated those that displayed prominent knickpoints.

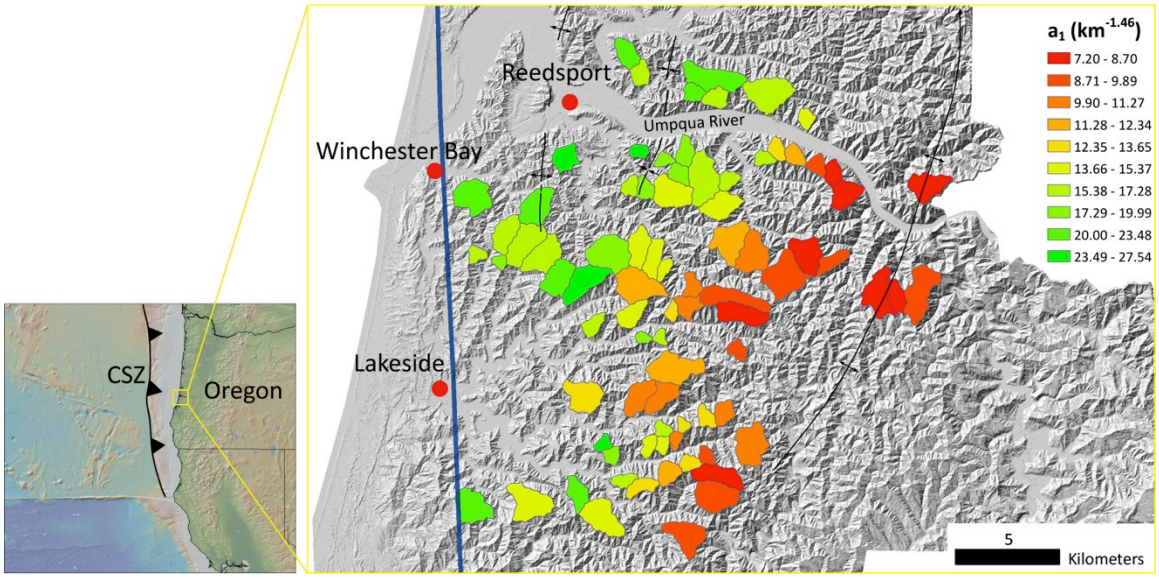

Figure 3: Regional Map. Our study area is located just north of Coos Bay along the Oregon Coast. Major towns are labeled and shown in red. Our study catchments are represented by polygons with coloration indicative of the best fitting a_1 value using a fixed a_2 of 0.73. There are no major faults in this area and all major folds are shown. Folds are gentle and are not believe to directly influence topography. The blue line is the surface projection of the -20 km downdip contour of the subducting slab from McCrory et al. (2004).

We examined the distributions of a_1, a_2, and s_0 to determine the extent to which each of the parameters vary between the catchments of our study group. Since the units of a_1 are dependent upon the value of a_2, we used a reference value approach similar to that used in numerous studies of normalized channel steepness in order to compare a_1 values between our study catchments (Duvall et al., 2004; Kirby and Whipple, 2001; Lague et al., 2000; Snyder et al., 2000). Following Wobus et al. (2006a), we determined the reference a_2 value to be the regional average of our set of catchment a_2 values. We then refit catchment slope-area data with the same empirical function, but with a fixed a_2 value equivalent to our reference value.

4.2. Correlating Erosion Rate to Morphology

We estimated erosion rates from six cosmogenic radionuclide (CRN) samples (five previously unpublished samples collected by J. Roering and J. Marshall and one from Heimsath et al. (2001)) from channel sediment using the CRONUS online calculator (Balco et al., 2008) (see Appendix B and Table 2 for additional details). Each sample integrates erosion rate information over the upstream drainage area from the sample location, which in our case is less than 10 km^2 for all samples. After erosion rate estimates were calculated, we fit the slope-area data from the corresponding catchment valley networks with the empirical slope-area relation, including our determined reference a_2 value. We proceeded to take the resulting best-fit a_1 values and obtained a power law relationship between a_1 and erosion rate for these catchments. To account for the error in each of the CRN-derived erosion rate estimates, we used an inverse-variance weighting scheme when fitting. Using this relationship, we were then able to produce

erosion rate estimates for all catchments in our study group. Under the assumption that the OCR is in steady-state equilibrium over the integration timescale of the CRN erosion rate estimates, we interpreted these erosion rate predictions to reflect long-term uplift rate (DiBiase et al., 2010).

5. Results

Fitting the empirical model of Stock and Dietrich (2003) to the 83 catchments in our study group generate average parameter values (mean ± SD) of 0.626 ± 0.091, 15.5 ± 6.4 km^{-2a_2}, and 0.732 ± 0.079 for s_0, a_1, and a_2, respectively (Figure 4). The a_1 distribution is very dispersed compared to the distributions of s_0 and a_2 with a coefficient of variation (mean/SD) of 0.41 compared to 0.15 and 0.11, respectively. This distribution of a_1 does, however, contain values with conflicting units due to the dependence of the units of a_1 on the corresponding best fitting a_2. The relative insensitivity of s_0 agrees with the hypothesis of Stock and Dietrich (2003) that valley slopes at small drainage areas are controlled by threshold-driven shallow landslides. Given that a_2 is also fairly consistent throughout the study group, we are confident that taking a reference a_2 approach is appropriate in this case in order to produce a_1 values with consistent units. Maintaining a fixed reference a_2 value of 0.73, we refit the empirical slope-area function to all of our catchments. This resulted in average parameter values (mean ± SD) of 0.624 ± .091 and 14.8 ± 4.9 $km^{-1.46}$ and for s_0 and a_1, respectively (Figure 4). The corresponding coefficients of variation for s_0 and a_1 for these reference a_2 fits are 0.15 and 0.33, respectively.

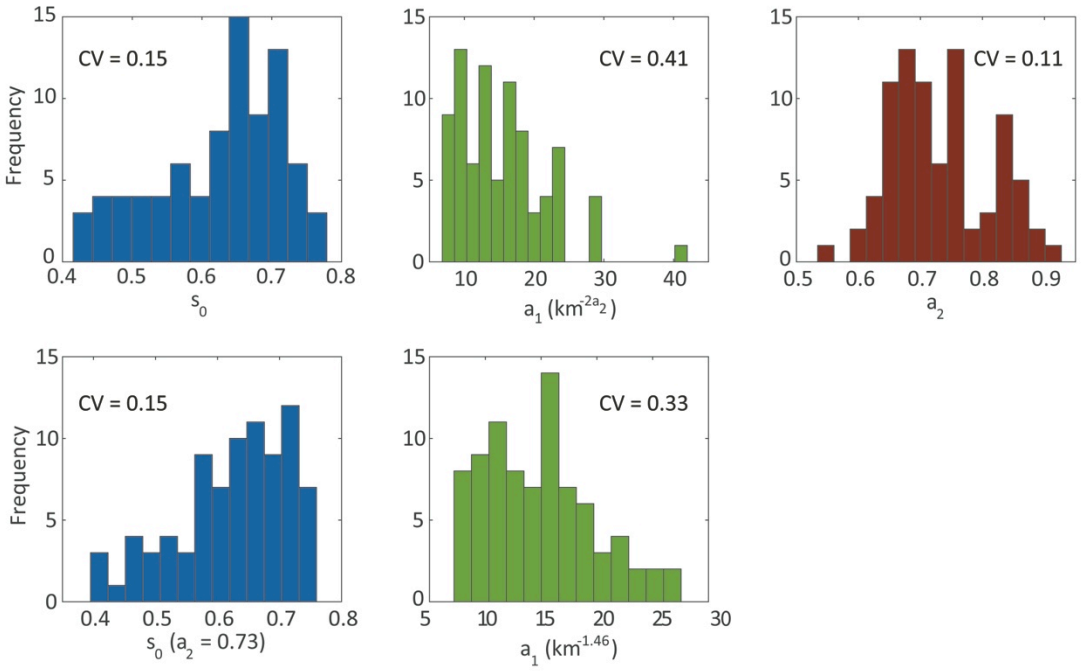

Figure 4: Parameter Distributions. The top row of distributions represents the best fitting parameters (s_0, a_1, and a_2) for the 83 catchments in this study. The bottom row of distributions represents the best fitting parameters (s_0 and a_1) for model fits with a fixed a_2 of 0.73.

We proceeded to fit the following power law to the catchment averaged erosion rate estimates and their corresponding best-fit a_1 parameters, with $a_2 = 0.73$:

$$E = p_1 a_1^{p_2}$$

, where E is in units of (mm/yr) and a_1 is in units of (km$^{-1.46}$) and the best fitting values for p_1 and p_2 were 0.328 mm/yr/km$^{0.524}$ and -0.359, respectively (Figure 5). The value of p_1 in this case represents the erosion rate for a catchment with an a_1 value of 1.0 km$^{-1.46}$, while p_2 controls the how sensitive erosion rate is to variations in a_1 and serves as the power law slope in log-log space. Therefore, increasingly negative values of p_2 suggest that erosion rates are more sensitive to differences in a_1, and the opposite case is true for less negative p_2 values.

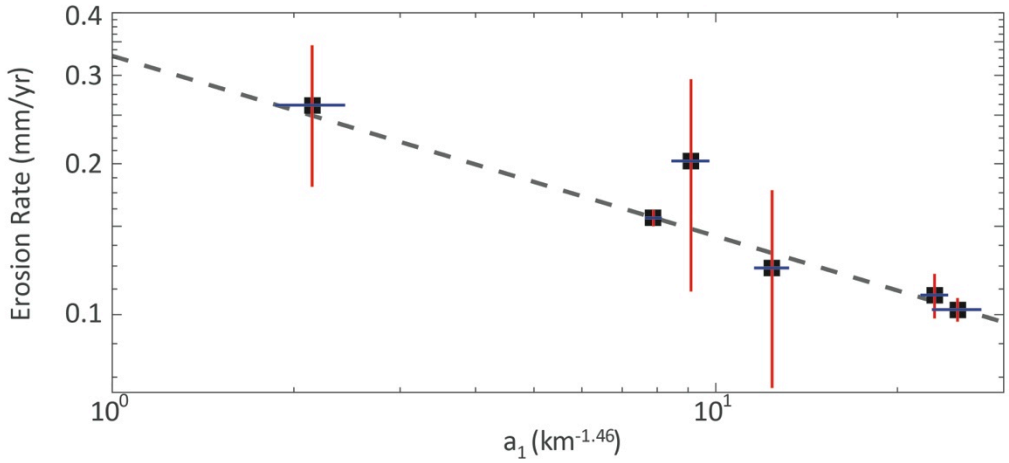

Figure 5: Erosion Rate Function. Black squares represent cosmogenic nuclide derived erosion rates and the associated best fitting a_1 values (a_2=0.73). Error bars extend one standard error away from the mean value. The black dashed line is the best fit power law relationship, which we then use to make estimates of long-term uplift rate for our study catchments.

Since cosmic rays penetrate to depths of ~0.6m in rock and estimated erosion rates for the OCR range from ~0.1 – 0.2 mm/yr, the estimated integration timescales of these erosion rates are on the order of 10^3-10^4 years (DiBiase et al., 2010). Under the assumption that the OCR has been in a state of topographic steady state over these timescales, we interpret predicted erosion rates from this function as predicted uplift rates over the same timescales. By applying this function to the best-fit a_1 values of the catchments in our study group, we produced a map of long-term uplift rate predictions to display potential spatial patterns. Our results indicate that long-term uplift rates increase inland from the coastline since a line fit to the long-term uplift rate estimates against distance from the -20 km downdip contour of McCrory et al. (2004) results in a statistically significant trend ($p<0.00001$).

6. Application to the OCR and CSZ

Convergent margins, such as the Cascadia Subduction Zone (CSZ), are typically associated with the occurrence of large magnitude earthquakes ($>M_w = 8$) as a consequence of plate subduction [e.g. Tohoku 2011(M_w 9.0), Sumatra 2004 (M_w 9.1), Alaska 1964 (M_w 9.2), Chile 1960 (M_w 9.5)]. The dynamic processes that lead to these large subduction zone earthquakes are thought to be cyclical in nature although no single subduction zone has been geodetically monitored long enough to record a complete cycle (Thatcher, 1984). The concept of an earthquake cycle was first proposed by Reid (1910) as part of elastic-rebound theory, which suggests that earthquakes are the result of the release of elastic strain energy that accumulates during interseismic periods. Thatcher (1984) observed that there are at least two regimes of permanent deformation related to interactions at subduction zones: a zone of "coseismic overshoot" close to the trench where coseismic vertical displacement of the overlying plate is positive (up), and a zone of "unrecovered interseismic straining" that occurs further inland where coseismic vertical displacement is negative (down) (Figure 6). This zone of unrecovered strain experiences the greatest magnitude of coseismic vertical displacement near the surface expression of the down-dip limit of the coseismic fault and decreases in magnitude gradually inland (Thatcher, 1984). Wherever the accumulated vertical strain is greater than the vertical strain released during coseismic displacement, net rock uplift can be imagined to have occurred.

While subduction zone earthquakes are not uncommon, there is no observational evidence or record of a large CSZ earthquake because European-American settlement in the Pacific Northwest is relatively recent. There is substantial indirect evidence for

several large magnitude events in Cascadia over the past ~6700 years (Witter et al., 2003). The most recent large magnitude earthquake to occur along the CSZ is thought to have been a ~M_w 9.0 event that ruptured the entire length of the subduction zone on January 26, 1700 AD, according to historical documentation of a tsunami that struck Japan as well as radiocarbon dating of buried trees and grass from onshore tsunami deposits in coastal Washington (Atwater and Yamaguchi, 1991; Satake et al., 1996). Additional buried marshes and forests in coastal Washington and Oregon are thought to be reflective of multiple episodes of coseismic subsidence and corresponding tsunamis, which inundated coastal regions and rapidly deposited sediment (Atwater, 1987; Darienzo and Peterson, 1990; Nelson and Personius, 1991). The presence of multiple buried soils, as well as an extensive record of seismically initiated turbidite deposits, indicate the occurrence of multiple previous subduction earthquakes of similar magnitude and frequency. Witter et al. (2003) recognized twelve buried soils at the Coquile River estuary that represent events of coseismic subsidence over the past 6500-6720 years, leading to an average recurrence interval of 570-590 years. An examination of buried soils at Yaquina Bay by Graehl et al. (2015) produce an estimate of recurrence interval of 420-580 years. Dating of offshore turbidite deposits, believed to have been triggered by coseismic shaking, produced recurrence interval estimates between 500-530 years for full-margin rupture events (Goldfinger et al., 2012). Not every subduction earthquake leads to a full-margin rupture since large magnitude earthquakes can result from localized rupture along segments of the plate interface. Goldfinger et al. (2012) used local turbidite records to determine additional recurrence intervals for these localized ruptures of segments along the CSZ. After accounting for the occurrence of both full-margin and

localized rupture related events, the corresponding recurrence interval of subduction earthquakes along the central Oregon Coast is 300-380 years (Goldfinger et al., 2012). In addition to large magnitude megathrust events, there exists a considerable amount of earthquake activity in the form of offshore and onshore crustal earthquakes in both the North American and Juan de Fuca plates. However, these events tend to be of much lower magnitudes and cannot account for the onset and correlation of buried soils and turbidite deposits along coastal Washington and Oregon (Clague, 1997). Additionally, there is no crustal structural feature that can account for temporal agreement of coseismic subsidence along the Cascadia margin (Clague, 1997).

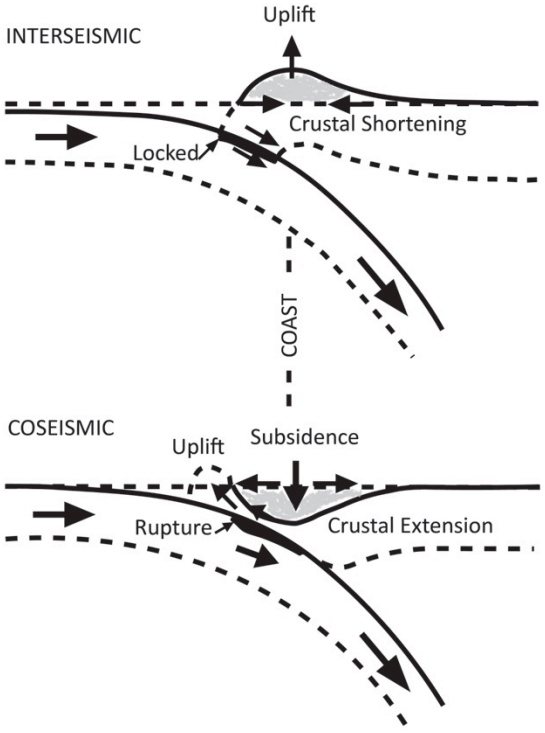

Figure 6: Subduction Zone Profile. Modified from Clague (1997). During interseismic periods, accumulated strain results in crustal shortening and uplift in the upper plate near the coast. When a great earthquake occurs, elastic strain is recovered and crustal extension and subsidence results. A zone of interseismic uplift and coseismic subsidence at the coast is shown in grey.

To demonstrate a potential application of debris flow valley profile morphology analysis, we used our estimates of long-term uplift rates for OCR debris flow catchments, in conjunction with estimated recurrence intervals and measured interseismic uplift rates, to provide estimates of coseismic subsidence for large subduction zone earthquakes. We assume that subduction earthquakes are periodic with respect to a constant recurrence interval and that the measured interseismic uplift rates are constant throughout each interseismic period and over past cycles. The total amount of uplift accumulated during the interseismic period can be expressed with the following equation:

$$\Delta z_I = U_I T_R$$

where Δz_I is the surface uplift due to a constant interseismic uplift rate, U_I, over a subduction earthquake recurrence interval of T_R. We interpreted the rate of long-term permanent deformation to be reflected by long-term uplift rates in the Oregon Coast Range, which results from inelastic vertical strain accumulation in each period of the earthquake cycle. The amount of net uplift accumulated after accounting for coseismic subsidence is expressed by a similar equation:

$$\Delta z_{LT} = U_{LT} T_R$$

, where Δz_{LT} is the net surface uplift from a complete earthquake cycle and U_{LT} is the long-term uplift rate. Subtracting Δz_{LT} from Δz_I results in the coseismic subsidence for a characteristic subduction zone earthquake. Combining the above equations, we can write the coseismic subsidence (Δz_C) as:

$$\Delta z_C = T_R(U_I - U_{LT})$$

allowing us to input various recurrence interval estimates, current interseismic uplift rates, and our debris flow profile derived long-term uplift rates to calculate a suite of spatially variable coseismic subsidence estimates.

Interseismic uplift rates were obtained from the dataset of Burgette et al. (2009), who used leveling and tidal gauge records to investigate the pattern of locking along the CSZ plate interface. Their measured interseismic uplift rates along the Oregon Coast and in the OCR are typically an order of magnitude greater than estimated long-term uplift rates, greatest at the coast, and decrease inland, eventually approaching values consistent with long-term uplift rate estimates. While there is significant along-strike (N-S) variation in interseismic uplift rate along the Oregon Coast, we focused on the Central Oregon Coast dataset of Burgette et al. (2009), which lacks significant along-strike variability and contains W-E transects of measurements taken near South Bay and Charleston in addition to a N-S survey along the coastline bounded by these transects. This Central Oregon Coast subset overlaps spatially with our study catchments, enabling us to compare W-E variations in interseismic and long-term uplift rate estimates. We plotted these measurements of interseismic uplift rate, as well as our long-term uplift rate estimates, as a function of the distance from surface projection of the -20 km downdip contour of the subducting slab, in order to maintain consistency with the geophysical observations of (Burgette et al. (2009)). Furthermore, we fit an exponential function to the plotted interseismic uplift rates and a linear function to the long-term uplift rate estimates in order to compare the inland variation of interseismic uplift rate with that of long-term uplift rates (Figure 7ab). When fitting the interseismic uplift rates, we subsampled data points taken from the N-S coastal survey of the Central Oregon Coast in

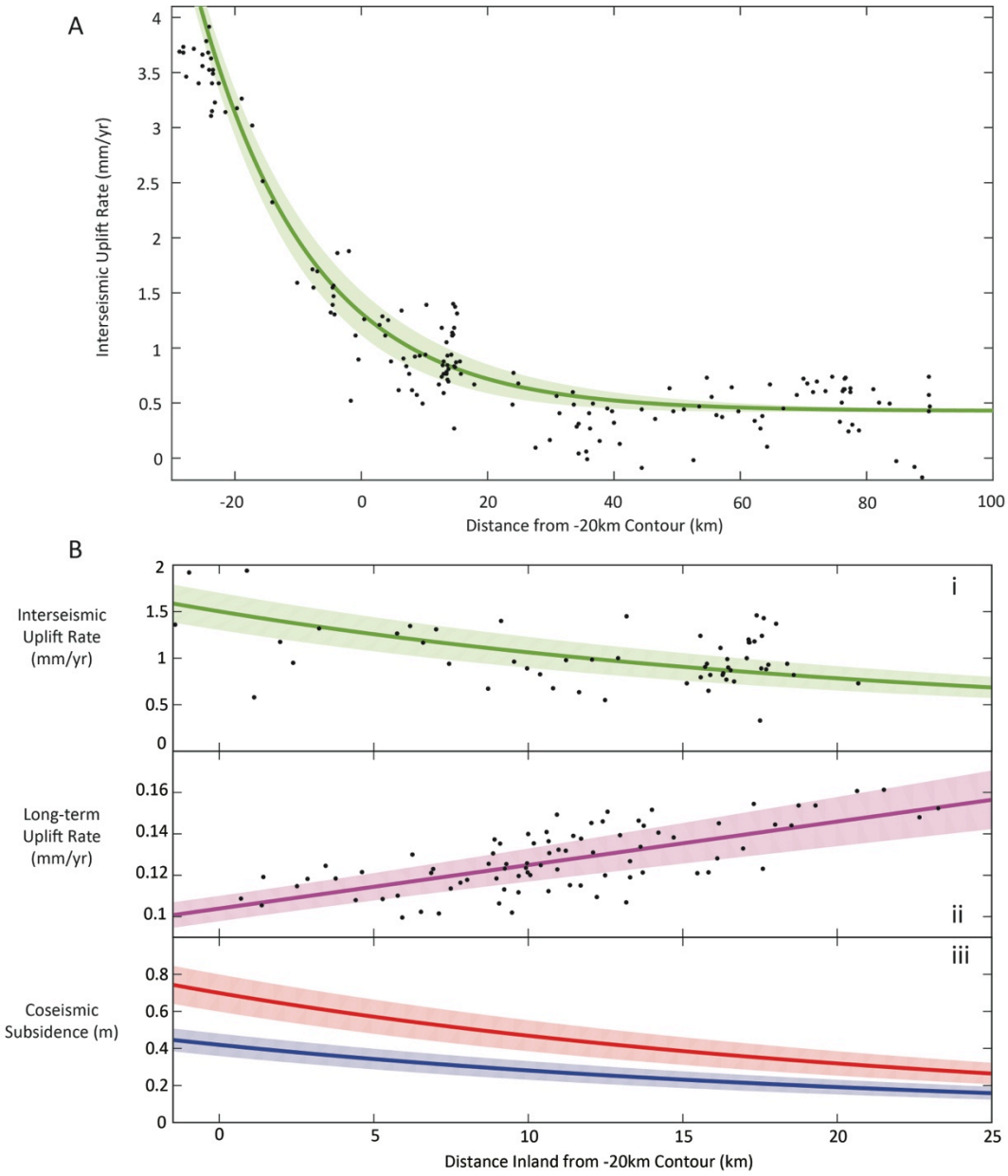

Figure 7: Inland Variation Plots. A: Interseismic uplift rates plotted against distance from the -20km contour. Black dots represent measurements with the green line the best-fit exponential function to the central coast data from Burgette et al. (2009). The shaded region represents the 95% CI of the fit. This represents only the portion of the central coast data that overlaps with our study area. **B:** i.) A subset from A focusing on the interseismic uplift rates within the study area. ii.) Catchment debris flow profile derived long-term uplift rates v. distance from the -20 km contour. Black dots represent the raw values obtained by using the erosion rate function from Figure 5 and assuming steady state. The shaded region represents the 95% CI of the trendline. iii.) Coseismic subsidence estimates using the best-fit trends from A and B and subduction earthquake recurrence intervals of 300 (blue) and 500 (red) years. Shaded regions are 95% CIs.

order to eliminate a sampling bias when fitting our exponential function. Additionally, we weighted both fits using the same inverse-variance weighting scheme used to fit the erosion rate prediction function.

By subtracting the long-term uplift rate function from the interseismic uplift rate function, we produced plots of the corresponding estimates of coseismic subsidence for a range of subduction zone earthquake recurrence intervals (Figure 7b). In all of our plots, coseismic subsidence is highest near the coast and decreases inland, consistent with the model predictions of Hyndman and Wang (1995) and Dragert et al. (1994). Coseismic subsidence estimates for the central Oregon Coast directly above the -20 km slab contour are 0.420 ± 0.060 m, 0.559 ± 0.080 m, and 0.70 ± 0.10 m (mean with 95% CI) for recurrence intervals of 300, 400, and 500 years. Historical subduction zone earthquakes in Alaska, Chile, and Japan had corresponding zones of coseismic subsidence, extending parallel to the subduction zones, which were approximately as wide as the zone of rupture (Ando, 1975; Plafker, 1969; Plafker and Savage, 1970; Thatcher, 1984). This indicates that the consideration of recurrence intervals corresponding to local subduction zone ruptures, rather than just entire-margin ruptures, might give a more accurate estimate of coseismic subsidence.

7. Discussion

Debris flows play a vital role in unglaciated steepland landscapes, transporting material derived from hillslopes and lowering reaches that lie above the channelized network. Additionally, valleys scoured by debris flows account for over 80% of the length of the valley network in large steepland basins (Stock and Dietrich, 2003). By

developing a method to extract information on local base level from the longitudinal profiles of these reaches, a large portion of the landscape that has previously largely been eschewed can be exploited to make inferences on patterns of uplift rate and lithologic and climate variations. Furthermore, current earthquake records in the Pacific Northwest are too short to accurately describe the deformation associated with Cascadia subduction zone earthquakes. Debris flow valley profiles have the potential to preserve long-term uplift rates over 10^4 year timescales and are abundant throughout the Oregon Coast Range. Since the long-term uplift history of the Coast Ranges represents an integral effect of CSZ related deformation, debris flow valley derived uplift rates could help constrain physical models by providing field derived evidence of the long-term effects of the subduction earthquake cycle.

Our analysis of debris flow valleys only takes into consideration the upper most portion of the valley network where debris flows traverse and scour the valley floor, eventually depositing the accumulated material at slopes of 0.03-0.1. These slopes typically coincide with the scaling break between slope and drainage area and are occupied by transitional reaches where debris flow runouts and long-term fluvial features can be found (Stock and Dietrich, 2003). By selecting a minimum slope threshold of 0.03, we ensure that our analyses capture the entire debris flow dominated portion of the network as well as the transitional reaches where debris flow deposits are found.

7.1. Debris Flow Parameters

There does not appear to be a strong correlation between any of the parameters and drainage area. While a_1 and s_0 do not have significant trends ($p = 0.068$ and $p = 0.61$,

respectively), a_2 decreases with drainage area (slope = -2.47E-8 m^{-2}, p = 0.0021). Given that we fix a_2 in our analyses, this trend should not influence our results in any way. Furthermore, to ensure that the choice of the fixed a_2 did not influence the results, we conducted a sensitivity analysis by fitting several versions of the empirical slope-area function with extreme fixed a_2 values to our catchment derived data. Since a_2 ranges from 0.495 to 0.927 in our study group, we repeated our fixed a_2 analysis using fixed values of 0.5 and 0.9 to see if the spatial pattern of long-term uplift rate estimates changed. We compared the resulting a_1 value datasets with each other (a_1 calculated for fixed a_2 of 0.5, 0.73, and 0.9) and the three datasets were very well correlated with each other, indicating that no information on the relative degree of slope-area curvature is lost due to the choice of the fixed a_2 (Figure 8). We also used the best-fitting erosion rate functions for a_1 values with fixed a_2 values of 0.5 and 0.9 to create two new sets of long-term uplift rate estimates for the catchments. We then ran linear regressions of these long-term uplift rate datasets against distance from the -20 km contour and conducted two-sample t-tests to determine whether the trends were significantly different. The resulting regression slopes relating distance from the -20km contour to long-term uplift rate were not significantly different from each other and from the original regression slope from our analysis using a fixed a_2=0.73 ($p>0.85$ for all comparisons). Additionally, the y-intercepts for the linear regressions with fixed a_2 values of 0.5 and 0.9 were both 0.1038 mm/yr, which compares to the value from our original regression (a_2=0.73) of 0.1039 mm/yr. Due to the nature of the empirical function, a_2 will always influence a_1 as it serves as a boundary condition by determining the trajectory of the curved, debris flow dominated portion of the network. However, the choice of a reference a_2 does not seem to influence the results of our study.

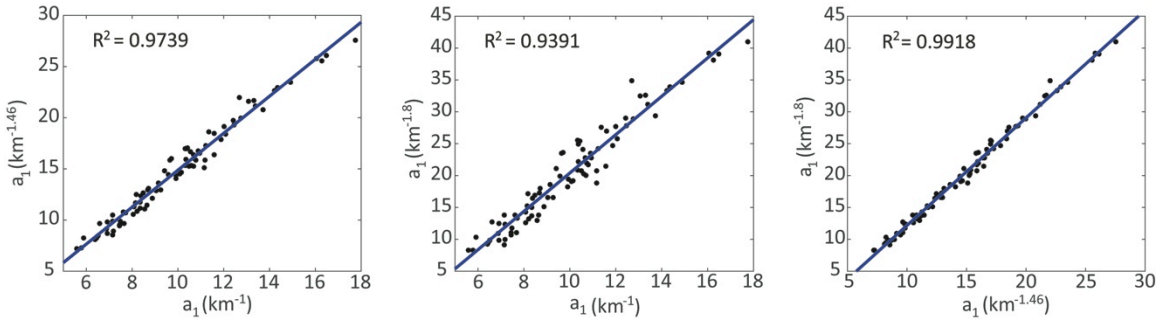

Figure 8: a_1 Comparisons. Different sets of a_1 values using different fixed values of a_2 are very well correlated. This indicates that choice of the fixed a_2 value used in our analysis should not inflence the results.

7.2. Uplift Rates and CSZ Deformation

While our calculated trend in long-term uplift rate with distance from the -20 km contour is statistically significant at the 95% confidence level, there are only a few data points gathered from catchments near the coast and from distances greater than 20 km from the -20 km contour. Near the coast the prevalence of debris flows vanishes, presumably due to low long-term uplift rates (<0.1 mm/yr) that result in shallower valley slopes. Additionally, marine terraces near the coast disrupt the uniform valley-ridge OCR morphology that is typical of inland catchments. Meanwhile, the inland extent of our study region is limited by the current availability of high-resolution lidar data of the OCR. While DOGAMI and NSF have done a tremendous job in making data available and have helped ensure that Oregon is one of the leading states in terms of lidar coverage, there are still large voids in many areas that are key to this work. This eastern limit of the lidar coverage area prevented our estimates of long-term uplift rates from extending inland more than 25 km from the -20 km downdip contour of McCrory et al. (2004). Applying our erosion rate proxy to additional inland catchments would have enabled us

to determine the inland extent of the increasing trend in long-term uplift. This is especially important as this trend may be reflective of relative sea level fluctuations due to the earthquake deformation cycle. For a catchment that subsides during a subduction zone earthquake, relative sea level rises and raises the local base level, possibly inundating previously incised valley floors. This would severely inhibit the ability of the network to incise and would reduce incisional efficiency until base level falls to an appropriate level due to interseismic uplift. The degree to which incision is inhibited may be related to the proportion of the interseismic cycle where higher order valleys are inundated. Furthermore, this trend might indicate that greater permanent vertical deformation may occur inland from the coast over multiple earthquake deformation cycles.

Permanent deformation and uplift along convergent margins has been attributed to deep-seated flow, underplating, and/or aseismic shortening within the accretionary wedge (Pavlis and Bruhn, 1983; Personius, 1995). Despite evidence indicating that the Oregon Coast Range is undergoing steady, constant long-term uplift, our results indicate that the rate of long-term uplift decreases at the coast despite an absence of major structure. Over this same region, interseismic uplift rates tend to increase near the coast, indicating a potential transition of dominant uplift processes. At the coast, interseismic uplift rates that are an order of magnitude greater than the long-term rates, as well as field evidence of coseismic subsidence associated with large magnitude subduction zone earthquakes, indicate that subduction earthquake cycle driven deformation controls the long-term rate of rock uplift (Figure 9). Further inland, interseismic uplift rates approach the long-term rates, indicating that there is minimal surface elevation change during megathrust

earthquakes. We attempted to estimate the inland extent of coseismic subsidence using the current uplift rates and our debris flow profile-based long-term rates, but the eastern limit of the lidar coverage area prohibited us from estimating the inland extent of this transition.

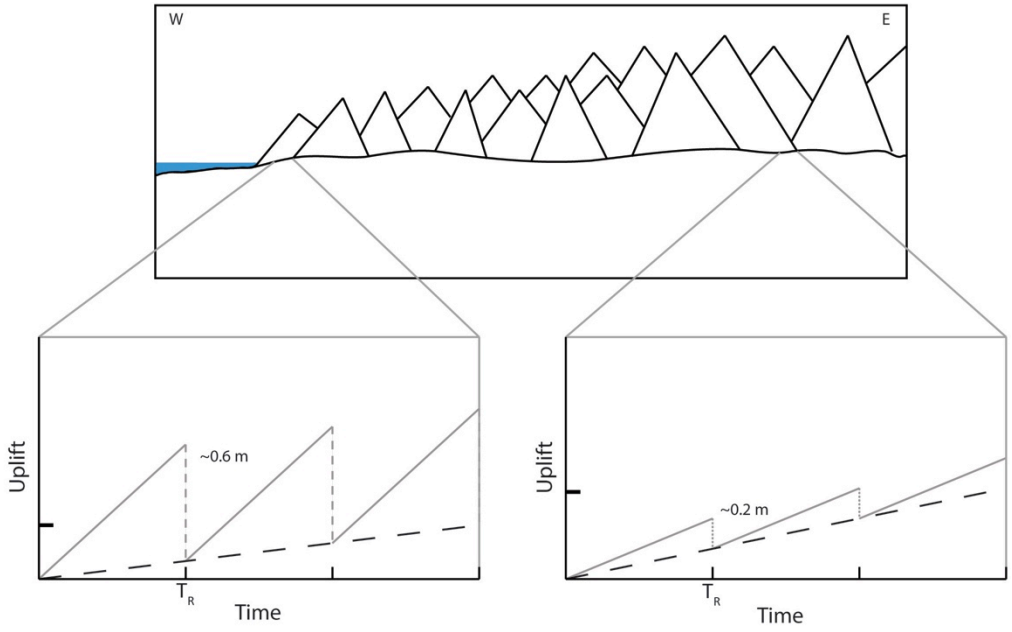

Figure 9: Subduction Zone Influence Hypothesis. Near the coast, interseismic uplift rates are high but long-term rates are low, indicating a potential dominance of earthquake deformation cycle related processes on topography. Inland from the coast, interseismic uplift rates approach the long-term rates, indicating that coseismic subsidence is approaching zero and therefore the influence of the earthquake deformation cycle on topography is minimal. Labeled values are approximate coseismic subsidence estimates for each earthquake cycle.

We compared our estimates of coseismic subsidence with previous measurements made from buried soils. Leonard et al. (2004) aggregated several estimates of coastal coseismic subsidence from previous studies of buried marshes and found that coseismic subsidence ranged from 0-2 m along Cascadia. For sites that overlap with our study area

(Umpqua and Coos Bay) coseismic subsidence estimates are 0.46 ± 0.31 m and 0.61 ± 0.32 m (mean ± standard deviation), respectively (Briggs, 1994; Darienzo and Peterson, 1995; Nelson, 1992; Nelson et al., 1996; Nelson et al., 1998; Peterson and Darienzo, 1989). Our estimates of coseismic subsidence at the -20 km contour, which approximates the coastline, are all in agreement with these observed values.

While our results agree with observed values of coseismic subsidence and suggest that topographic analysis can be a useful tool for making estimates, we make several assumptions that oversimplify subduction earthquake dynamics. Wang et al. (2012) provided a more detailed description of the subduction earthquake cycle, where afterslip along the fault as well as viscoelastic relaxation of the mantle occur prior to relocking. Since these processes have never been observed along the CSZ, it is difficult to determine what their influence on coastal uplift is and if they contribute to the long-term pattern of uplift in the OCR. These processes are, however, believed to occur over timescales of a few months to a few years with fault locking occurring over the vast majority of the interseismic period (Wang et al., 2012). Given that the measured uplift rates of Burgette et al. (2009) represent a snapshot of the interseismic period, we are also unsure if these rates remain constant or if they change over time from cycle to cycle or even within a single interseismic period. While slip along the plate interface may be constant over time, this does not imply that the deformation rate has also been held constant due to changing geometries over the earthquake cycle. Subduction dynamics is an area of active research and given that observations of the subduction earthquake cycle are limited, it is difficult to constrain all aspects of earthquake related deformation along active margins.

Therefore, it is difficult to confirm or refute the existence of periodic, characteristic events that have the potential to influence the OCR landscape in a predictable way.

8. Conclusion

Surface deformation along the Oregon coast is due to the long-term effects of multiple subduction earthquake cycles, however current earthquake records are too short to accurately describe this deformation (Personius, 1995). Given that the Oregon Coast Range is presumed to exist in a relatively steady state, the corresponding valley networks may be able to preserve information on deformation over multiple cycles, which may give greater insight to the long-term effects of subduction dynamics from interpretations of surface topography. Since debris flow valleys account for the vast majority of network length in the Oregon Coast Range, we developed a method using a previously proposed empirical relation between valley slope and upstream drainage area for debris flow valleys to relate profile form to long-term uplift rate. Our results indicate that there may be a trend of increasing long-term uplift rate inland from the coast in the central OCR, reflecting increased magnitudes of vertical inelastic strain accumulation over multiple subduction earthquake cycles. This contrasts with the pattern of elastic deformation seen during interseismic periods, where uplift rates are typically highest at the coast and decrease inland. Using subduction megathrust earthquake recurrence interval estimates in conjunction with the inland patterns of interseismic and long-term uplift rates, we were able to produce a spatial pattern of expected coseismic subsidence that extended further inland than previous field based measurements. This application demonstrates that the

shape of debris flow valley profiles in steepland regions may be used to help constrain models of subduction zone dynamics.

APPENDIX A

TABLE OF PARAMETERS AND VARIABLES

Table 1: Table of Parameters and Variables.

Parameter	**Name**	**Units**
a_1	Concavity Coefficient	$(\text{length})^{-2a_2}$
a_2	Fluvial Exponent	Unitless
K	Coefficient of Erosion	$(\text{length})^{1-2m}(\text{time})^{-1}$
k_s	Channel Steepness Index	(length)
m	Area Scaling Exponent	Unitless
n	Slope Scaling Exponent	Unitless
s_0	Ideal Valley Head Slope	(length/length)
θ	Concavity Index	Unitless

Variable	**Name**	**Units**
A	Upstream Drainage Area	$(\text{length})^2$
E	Vertical Erosion Rate	(length)/(time)
S	Channel (Valley) Gradient	(length/length)
T_R	Subduction Earthquake Recurrence Interval	(time)
U_I	Interseismic Uplift Rate	(length)/(time)
U_{LT}	Long-term Uplift Rate	(length)/(time)
Δz_C	Coseismic Subsidence	(length)
Δz_I	Interseismic Elevation Change	(length)
Δz_{LT}	Earthquake Cycle Elevation Change	(length)

APPENDIX B

CRN DERIVED EROSION RATE ESTIMATES

The cosmogenic radionuclide-derived erosion rates used to calibrate the functional relationship with a_1 were derived from one published and five previously unpublished stream sediment samples. Beryllium-10 concentrations were obtained for all samples except for the sample from Heimsath et al. (2001), for which aluminum-26 concentration was measured. We used the CRONUS online calculator to calculate catchment-averaged surface erosion rates (Balco et al., 2008). Table 2 contains relevant information for the six samples used in this study. Samples CRN 501 and CRN 502 correspond to non-overlapping areas of the Sullivan Creek catchment. Sample Stream B-R corresponds to a region that overlaps with the regions described by CRN 501 and CRN 502 and a mixing relationship was used to derive the erosion rate for the downstream area corresponding only to sample Stream B-R (Granger et al., 1996). Errors are 1σ propogated from Accelerator Mass Spectrometry (AMS).

Table 2: CRN Sample Analyses. Samples of cosmogenic radionuclide concentrations derived from stream sediment in the Oregon Coast Range. Concentrations were obtained using AMS and the CRONUS calculator was used to make erosion rate estimates.

Sample	Location (Decimal Degrees)	Concentration (atoms g^{-1} quartz)	Error (atoms g^{-1} quartz)	Erosion Rate (mm/yr)	Error (mm/yr)	Notes
CRN 500	Upper Smith River (-123.811°, 43.964°)	70902.91 (^{10}Be)	3408.59	0.1023	0.0049	Collected by Josh Roering (JR) and Jill Marshall (JM)
CRN 501	Sullivan Creek (-124.105°, 43.470°)	53211.86 (^{10}Be)	22369.24	0.124	0.052	Collected by JR and JM
CRN 502	Sullivan Creek (-124.104°, 43.468°)	56073.93 (^{10}Be)	5376.31	0.109	0.011	Collected by JR and JM
CRN 503	Franklin Creek (-123.905°, 43.670°)	44164 (^{10}Be)	2592	0.1559	0.0049	Collected by JR and JM
HadsCRN	Hadsall Creek (-123.824°, 43.985°)	33766.10 (^{10}Be)	4666.26	0.203	0.091	Collected by JR and JM
Stream B-R	Sullivan Creek (-124.113°, 43.469°)	287899 (^{26}Al)	89864	0.262 (0.165)	0.081 (0.066)	Heimsath et al. (2001), values in parentheses are raw values before mixing correction.

REFERENCES CITED

Ahnert, F., 1970. Functional relationships between denudation, relief, and uplift in large, mid-latitude drainage basins. American Journal of Science 268, 243-263.

Almond, P., Roering, J., Hales, T., 2007. Using soil residence time to delineate spatial and temporal patterns of transient landscape response. Journal of Geophysical Research: Earth Surface (2003–2012) 112.

Ando, M., 1975. Source mechanisms and tectonic significance of historical earthquakes along the Nankai Trough, Japan. Tectonophysics 27, 119-140.

Atwater, B.F., 1987. Evidence for great Holocene earthquakes along the outer coast of Washington State. Science 236, 942-944.

Atwater, B.F., Yamaguchi, D.K., 1991. Sudden, probably coseismic submergence of Holocene trees and grass in coastal Washington State. Geology 19, 706-709.

Balco, G., Stone, J.O., Lifton, N.A., Dunai, T.J., 2008. A complete and easily accessible means of calculating surface exposure ages or erosion rates from 10 Be and 26 Al measurements. Quaternary geochronology 3, 174-195.

Baldwin, E.M., 1956. Geologic map of the lower Siuslaw River area, Oregon.

Benda, L., 1990. The influence of debris flows on channels and valley floors in the Oregon Coast Range, USA. Earth Surface Processes and Landforms 15, 457-466.

Benda, L., Dunne, T., 1997. Stochastic forcing of sediment supply to channel networks from landsliding and debris flow. Water Resources Research 33, 2849-2863.

Beschta, R.L., 1978. Long‐term patterns of sediment production following road construction and logging in the Oregon Coast Range. Water Resources Research 14, 1011-1016.

Bierman, P., Clapp, E., Nichols, K., Gillespie, A., Caffee, M.W., 2001. Using cosmogenic nuclide measurements in sediments to understand background rates of erosion and sediment transport, Landscape Erosion and Evolution Modeling. Springer, pp. 89-115.

Binnie, S.A., Phillips, W.M., Summerfield, M.A., Fifield, L.K., 2007. Tectonic uplift, threshold hillslopes, and denudation rates in a developing mountain range. Geology 35, 743-746.

Briggs, G.G., 1994. Coastal crossing of the elastic strain zero-isobase, Cascadia margin, south central Oregon coast. Portland State University.

Burgette, R.J., Weldon, R.J., Schmidt, D.A., 2009. Interseismic uplift rates for western Oregon and along‐strike variation in locking on the Cascadia subduction zone. Journal of Geophysical Research: Solid Earth (1978–2012) 114.

Clague, J.J., 1997. Evidence for large earthquakes at the Cascadia subduction zone. Reviews of Geophysics 35, 439-460.

Cyr, A.J., Granger, D.E., Olivetti, V., Molin, P., 2010. Quantifying rock uplift rates using channel steepness and cosmogenic nuclide–determined erosion rates: Examples from northern and southern Italy. Lithosphere 2, 188-198.

Darienzo, M., Peterson, C., 1995. Magnitude and frequency of subduction-zone earthquakes along the northern Oregon coast in the past 3,000 years.

Darienzo, M.E., Peterson, C.D., 1990. Episodic tectonic subsidence of late Holocene salt marshes, northern Oregon central Cascadia margin. Tectonics 9, 1-22.

DiBiase, R.A., Whipple, K.X., Heimsath, A.M., Ouimet, W.B., 2010. Landscape form and millennial erosion rates in the San Gabriel Mountains, CA. Earth and Planetary Science Letters 289, 134-144.

Dietrich, W., Dunne, T., 1978. Sediment budget for a small catchment in a mountainous terrain.

Dietrich, W.E., Bellugi, D.G., Sklar, L.S., Stock, J.D., Heimsath, A.M., Roering, J.J., 2003. Geomorphic transport laws for predicting landscape form and dynamics. Prediction in geomorphology, 103-132.

Dragert, H., Hyndman, R., Rogers, G., Wang, K., 1994. Current deformation and the width of the seismogenic zone of the northern Cascadia subduction thrust. Journal of Geophysical Research: Solid Earth (1978–2012) 99, 653-668.

Duvall, A., Kirby, E., Burbank, D., 2004. Tectonic and lithologic controls on bedrock channel profiles and processes in coastal California. Journal of Geophysical Research: Earth Surface (2003–2012) 109.

Flint, J., 1974. Stream gradient as a function of order, magnitude, and discharge. Water Resources Research 10, 969-973.

Goldfinger, C., Nelson, C.H., Morey, a.E., Joel E, J., Patton, J., Karabanov, E., Gutierrez-Pastor, J., Eriksson, A., Gracia, E., Dunhill, G., Enkin, R., Dallimore, A., Valiier, T., 2012. Turbidite Event History — Methods and Implications for Holocene Paleoseismicity of the Cascadia Subduction Zone. U.S. Geological Survey Professional Paper 1661-F, 170 p.-170 p.

Graehl, N.A., Kelsey, H.M., Witter, R.C., Hemphill-Haley, E., Engelhart, S.E., 2015. Stratigraphic and microfossil evidence for a 4500-year history of Cascadia subduction zone earthquakes and tsunamis at Yaquina River estuary, Oregon, USA. Geological Society of America Bulletin 127, 211-226.

Granger, D.E., Kirchner, J.W., Finkel, R., 1996. Spatially averaged long-term erosion rates measured from in situ-produced cosmogenic nuclides in alluvial sediment. The Journal of Geology, 249-257.

Hack, J.T., 1973. Stream-profile analysis and stream-gradient index. Journal of Research of the US Geological Survey 1, 421-429.

Harkins, N., Kirby, E., Heimsath, A., Robinson, R., Reiser, U., 2007. Transient fluvial incision in the headwaters of the Yellow River, northeastern Tibet, China. Journal of Geophysical Research: Earth Surface (2003–2012) 112.

Heimsath, A.M., Dietrich, W.E., Nishiizumi, K., Finkel, R.C., 2001. Stochastic processes of soil production and transport: Erosion rates, topographic variation and cosmogenic nuclides in the Oregon Coast Range. Earth Surface Processes and Landforms 26, 531-552.

Heller, P.L., Dickinson, W.R., 1985. Submarine ramp facies model for delta-fed, sand-rich turbidite systems. AAPG Bulletin 69, 960-976.

Howard, A.D., 1997. Badland morphology and evolution: Interpretation using a simulation model. Earth Surface Processes and Landforms 22, 211-227.

Howard, A.D., Kerby, G., 1983. Channel changes in badlands. Geological Society of America Bulletin 94, 739-752.

Hurtrez, J.E., Sol, C., Lucazeau, F., 1999. Effect of drainage area on hypsometry from an analysis of small‐scale drainage basins in the Siwalik Hills (Central Nepal). Earth Surface Processes and Landforms 24, 799-808.

Hyndman, R., Wang, K., 1995. The rupture zone of Cascadia great earthquakes from current deformation and the thermal regime. Journal of Geophysical Research: Solid Earth (1978–2012) 100, 22133-22154.

Kelsey, H.M., Ticknor, R.L., Bockheim, J.G., Mitchell, E., 1996. Quaternary upper plate deformation in coastal Oregon. Geological Society of America Bulletin 108, 843-860.

Kirby, E., Ouimet, W., 2011. Tectonic geomorphology along the eastern margin of Tibet: insights into the pattern and processes of active deformation adjacent to the Sichuan Basin. Geological Society, London, Special Publications 353, 165-188.

Kirby, E., Whipple, K., 2001. Quantifying differential rock-uplift rates via stream profile analysis. Geology 29, 415-418.

Kirby, E., Whipple, K.X., 2012. Expression of active tectonics in erosional landscapes. Journal of Structural Geology 44, 54-75.

Kirby, E., Whipple, K.X., Tang, W., Chen, Z., 2003. Distribution of active rock uplift along the eastern margin of the Tibetan Plateau: Inferences from bedrock channel longitudinal profiles. Journal of Geophysical Research: Solid Earth (1978–2012) 108.

Koons, P.O., Kirby, E., 2007. The Role of Surface Processes in Fault Evolution. Tectonic Faults: Agents of Change on a Dynamic Earth 95, 205.

Lague, D., Davy, P., 2003. Constraints on the long‐term colluvial erosion law by analyzing slope‐area relationships at various tectonic uplift rates in the Siwaliks Hills (Nepal). Journal of Geophysical Research: Solid Earth (1978–2012) 108.

Lague, D., Davy, P., Crave, A., 2000. Estimating uplift rate and erodibility from the area-slope relationship: Examples from Brittany (France) and numerical modelling. Physics and Chemistry of the Earth, Part A: Solid Earth and Geodesy 25, 543-548.

Leonard, L.J., Hyndman, R.D., Mazzotti, S., 2004. Coseismic subsidence in the 1700 great Cascadia earthquake: Coastal estimates versus elastic dislocation models. Geological Society of America Bulletin 116, 655-670.

Lovell, J., 1969. Tyee Formation: a study of proximality in turbidites. Journal of Sedimentary Research 39.

Mackin, J.H., 1948. Concept of the graded river. Geological Society of America Bulletin 59, 463-512.

Marshall, J.A., Roering, J.J., 2014. Diagenetic variation in the Oregon Coast Range: Implications for rock strength, soil production, hillslope form, and landscape evolution. 1395-1417.

McCrory, P.A., Blair, J.L., Oppenheimer, D.H., Walter, S.R., 2004. Depth to the Juan de Fuca slab beneath the Cascadia subduction margin: A 3-D model for sorting earthquakes. US Department of the Interior, US Geological Survey.

McNeill, L.C., Goldfinger, C., Kulm, L.D., Yeats, R.S., 2000. Tectonics of the Neogene Cascadia forearc basin: Investigations of a deformed late Miocene unconformity. Geological Society of America Bulletin 112, 1209-1224.

Milliman, J.D., Syvitski, J.P., 1992. Geomorphic/tectonic control of sediment discharge to the ocean: the importance of small mountainous rivers. The Journal of Geology, 525-544.

Montgomery, D.R., Buffington, J.M., 1997. Channel-reach morphology in mountain drainage basins. Geological Society of America Bulletin 109, 596-611.

Nelson, A.R., 1992. Holocene tidal-marsh stratigraphy in south-central Oregon-Evidence for localized sudden submergence in the Cascadia subduction zone.

Nelson, A.R., Jennings, A.E., Kashima, K., 1996. An earthquake history derived from stratigraphic and microfossil evidence of relative sea-level change at Coos Bay, southern coastal Oregon. Geological Society of America Bulletin 108, 141-154.

Nelson, A.R., Ota, Y., Umitsu, M., Kashima, K., Matsushima, Y., 1998. Seismic or hydrodynamic control of rapid late-Holocene sea-level rises in southern coastal Oregon, USA? The Holocene 8, 287-299.

Nelson, A.R., Personius, S.F., 1991. The potential for great earthquakes in Oregon and Washington; an overview of recent coastal geologic studies and their bearing on segmentation of Holocene ruptures, central Cascadia subduction zone. US Geological Survey.

Ouimet, W.B., Whipple, K.X., Granger, D.E., 2009. Beyond threshold hillslopes: Channel adjustment to base-level fall in tectonically active mountain ranges. Geology 37, 579-582.

Pavlis, T.L., Bruhn, R.L., 1983. Deep‐seated flow as a mechanism for the uplift of broad forearc ridges and its role in the exposure of high P/T metamorphic terranes. Tectonics 2, 473-497.

Perron, J.T., Royden, L., 2013. An integral approach to bedrock river profile analysis. Earth Surface Processes and Landforms 38, 570-576.

Personius, S.F., 1995. Late Quaternary stream incision and uplift in the forearc of the Cascadia subduction zone, western Oregon. Journal of Geophysical Research: Solid Earth (1978–2012) 100, 20193-20210.

Peterson, C., Darienzo, M., 1989. Episodic, abrupt tectonic subsidence recorded in late Holocene deposits of the South Slough syncline: An on-land expression of shelf fold belt deformation from the southern Cascadia margin, Geological Society of America Abstracts with Programs, p. 129.

Plafker, G., 1969. Tectonics of the March 27, 1964, Alaska earthquake. US Government Printing Office.

Plafker, G., Savage, J., 1970. Mechanism of the Chilean earthquakes of May 21 and 22, 1960. Geological Society of America Bulletin 81, 1001-1030.

Reid, H.F., 1910. The mechanics of the earthquake. Carnegie institution of Washington.

Reneau, S.L., Dietrich, W.E., 1991. Erosion rates in the southern Oregon Coast Range: Evidence for an equilibrium between hillslope erosion and sediment yield. Earth Surface Processes and Landforms 16, 307-322.

Roering, J.J., 2008. How well can hillslope evolution models "explain" topography? Simulating soil transport and production with high-resolution topographic data. Geological Society of America Bulletin 120, 1248-1262.

Roering, J.J., Kirchner, J.W., Dietrich, W.E., 2001. Hillslope evolution by nonlinear, slope‐dependent transport: Steady state morphology and equilibrium adjustment timescales. Journal of Geophysical Research: Solid Earth (1978‐2012) 106, 16499-16513.

Roering, J.J., Kirchner, J.W., Dietrich, W.E., 2005. Characterizing structural and lithologic controls on deep-seated landsliding: Implications for topographic relief and landscape evolution in the Oregon Coast Range, USA. Geological Society of America Bulletin 117, 654-668.

Roering, J.J., Marshall, J., Booth, A.M., Mort, M., Jin, Q., 2010. Evidence for biotic controls on topography and soil production. Earth and Planetary Science Letters 298, 183-190.

Satake, K., Shimazaki, K., Tsuji, Y., Ueda, K., 1996. Time and size of a giant earthquake in Cascadia inferred from Japanese tsunami records of January 1700. Nature 379, 246-249.

Schwanghart, W., Scherler, D., 2013. Short Communication: TopoToolbox 2 – an efficient and user-friendly tool for Earth surface sciences. Earth Surf. Dynam. Discuss. 1, 261-275.

Snavely, P.D., Wagner, H.C., MacLeod, N.S., 1964. Rhythmic-bedded eugeosynclinal deposits of the Tyee formation, Oregon Coast Range. Kansas Geological Survey Bulletin 169, 461-480.

Snyder, N.P., Whipple, K.X., Tucker, G.E., Merritts, D.J., 2000. Landscape response to tectonic forcing: Digital elevation model analysis of stream profiles in the Mendocino triple junction region, northern California. Geological Society of America Bulletin 112, 1250-1263.

Snyder, N.P., Whipple, K.X., Tucker, G.E., Merritts, D.J., 2003a. Channel response to tectonic forcing: field analysis of stream morphology and hydrology in the Mendocino triple junction region, northern California. Geomorphology 53, 97-127.

Snyder, N.P., Whipple, K.X., Tucker, G.E., Merritts, D.J., 2003b. Importance of a stochastic distribution of floods and erosion thresholds in the bedrock river incision problem. Journal of Geophysical Research: Solid Earth (1978–2012) 108.

Stock, J., Dietrich, W.E., 2003. Valley incision by debris flows: Evidence of a topographic signature. Water Resources Research 39.

Stock, J.D., Dietrich, W.E., 2006. Erosion of steepland valleys by debris flows. Geological Society of America Bulletin 118, 1125-1148.

Thatcher, W., 1984. The earthquake deformation cycle, recurrence, and the time‐predictable model. Journal of Geophysical Research: Solid Earth (1978‐2012) 89, 5674-5680.

Tucker, G.E., Bras, R.L., 1998. Hillslope processes, drainage density, and landscape morphology. Water Resources Research 34, 2751-2764.

Wang, K., Hu, Y., He, J., 2012. Deformation cycles of subduction earthquakes in a viscoelastic Earth. Nature 484, 327-332.

Whipple, K.X., 2004. Bedrock rivers and the geomorphology of active orogens. Annu. Rev. Earth Planet. Sci. 32, 151-185.

Whipple, K.X., Tucker, G.E., 1999. Dynamics of the stream‐power river incision model: Implications for height limits of mountain ranges, landscape response timescales, and research needs. Journal of Geophysical Research: Solid Earth (1978–2012) 104, 17661-17674.

Whittaker, A.C., Cowie, P.A., Attal, M., Tucker, G.E., Roberts, G.P., 2007. Contrasting transient and steady‐state rivers crossing active normal faults: New field observations from the Central Apennines, Italy. Basin Research 19, 529-556.

Witter, R.C., Kelsey, H.M., Hemphill-Haley, E., 2003. Great Cascadia earthquakes and tsunamis of the past 6700 years, Coquille River estuary, southern coastal Oregon. Geological Society of America Bulletin 115, 1289-1306.

Wobus, C., Whipple, K.X., Kirby, E., Snyder, N., Johnson, J., Spyropolou, K., Crosby, B., Sheehan, D., 2006a. Tectonics from topography: Procedures, promise, and pitfalls. Geological Society of America Special Papers 398, 55-74.

Wobus, C.W., Hodges, K.V., Whipple, K.X., 2003. Has focused denudation sustained active thrusting at the Himalayan topographic front? Geology 31, 861-864.

Wobus, C.W., Whipple, K.X., Hodges, K.V., 2006b. Neotectonics of the central Nepalese Himalaya: Constraints from geomorphology, detrital 40Ar/39Ar thermochronology, and thermal modeling. Tectonics 25.